

KEK-TH-1462

Associated production of light gravitinos in e^+e^- and $e^-\gamma$ collisions

K. Mawatari^{1,a}, B. Oexl^{1,b}, Y. Takaesu^{2,c}

¹ Theoretische Natuurkunde and IIHE/ELEM, Vrije Universiteit Brussel, and International Solvay Institutes, Pleinlaan 2, B-1050 Brussels, Belgium

² KEK Theory Center, and Sokendai, Tsukuba 305-0801, Japan

the date of receipt and acceptance should be inserted later

Abstract. Light gravitino productions in association with a neutralino (selectron) in e^+e^- ($e^-\gamma$) collisions are restudied in a scenario that the lightest supersymmetric particle is a gravitino and the produced neutralino (selectron) promptly decays into a photon (electron) and a gravitino. We explicitly give the helicity amplitudes for the production processes by using the effective goldstino interaction Lagrangian, and present the cross sections with different collision energies and mass spectra. We also examine selection efficiencies by kinematical cuts and beam polarizations for the signal and background processes, and show that the energy and angular distributions of the photon (electron) can explore the mass of the t -channel exchange particle as well as the mass of the decaying particle at a future e^+e^- ($e^-\gamma$) collider.

1 Introduction

Gravitinos are spin-3/2 superpartners of gravitons in local supersymmetric extensions to the Standard Model (SM). Since the gravitino becomes massive via the super-Higgs mechanism, its mass is related to the scale of supersymmetry (SUSY) breaking as well as the Planck scale like

$$m_{3/2} \sim (M_{\text{SUSY}})^2 / M_{\text{Pl}}. \quad (1)$$

This implies that the gravitino can take a wide range of mass, depending on the SUSY breaking scale, from eV up to scales beyond TeV, and provide rich phenomenology in particle physics as well as in cosmology [1]. While the interactions of the helicity $\pm 3/2$ components of the gravitino are suppressed by the Planck scale, those of the helicity $\pm 1/2$ components are suppressed by the SUSY breaking scale if the gravitino mass is much smaller than the energy scale of the interactions, due to the goldstino equivalence theorem, and can be important even for collider phenomenology.

Gravitino productions in association with a SUSY particle are known processes which become significant at colliders when the mass of the gravitino is very light as $m_{3/2} \sim \mathcal{O}(10^{-2} \text{ eV})$ or less, since the cross sections are inversely proportional to the square of the gravitino mass

$$\sigma \propto 1/m_{3/2}^2. \quad (2)$$

Such a very light gravitino is suggested by the context of no-scale supergravity [2, 3] and some extra-dimensional

models [4], while typical gauge-mediated SUSY breaking (GMSB) scenarios expect a mass of 1 eV–10 keV [1]. Several studies on the associated gravitino productions have been performed so far, for instance, $\tilde{\chi}_1^0\tilde{G}$ productions in e^+e^- [5, 6, 7, 8] and hadronic [8] collisions, $\tilde{e}\tilde{G}$ productions in $e\gamma$ collisions [9], and $\tilde{g}\tilde{G}$ [10, 11, 12] and $\tilde{q}\tilde{G}$ [11, 12] productions in hadronic collisions. When the associated SUSY particle is the next-to-lightest supersymmetric particle (NLSP) and promptly decays into a SM particle and a LSP gravitino, the above production processes lead to particular collider signatures, such as $\gamma + \cancel{E}$, $e + \cancel{E}$, and $\text{jet} + \cancel{E}$, where the missing energy is carried away by two gravitinos, and these signals set mass bounds on the gravitino and the other SUSY particles. The current experimental bound on the gravitino mass from the single-photon plus missing-energy signal¹ in $\tilde{\chi}_1^0\tilde{G}$ associated productions is given by the LEP experiment as a function of the neutralino and selectron masses [13], e.g.

$$m_{3/2} \gtrsim 10^{-5} \text{ eV} \quad (3)$$

for $m_{\tilde{\chi}_1^0} = 140 \text{ GeV}$ and $m_{\tilde{e}} = 150 \text{ GeV}$. We note that the Tevatron also set a similar bound on the gravitino mass for the $\gamma + \cancel{E}$ [14] and $\text{jet} + \cancel{E}$ [15] channels, where it is assumed, however, that all SUSY particles except the gravitino are too heavy to be produced on-shell [16].

While the previous searches for gravitino productions have been somewhat restricted due to limitations of simulation tools, in the recent paper [17] implementation of the

^a e-mail: kentaro.mawatari@vub.ac.be

^b e-mail: bettina.oexl@vub.ac.be

^c e-mail: takaesu@post.kek.jp

¹ We note that a two-photon plus missing-energy signal, where the two photons come from two neutralino decays, does not provide any constraint on the gravitino mass.

spin-3/2 gravitino in MadGraph/MadEvent (MG/ME) [19, 20, 21] was reported, where new HELAS (HELicity Amplitude Subroutines) [18] codes were introduced to calculate helicity amplitudes with massive spin-3/2 gravitinos. They are implemented in such a way that amplitudes with external gravitinos can be generated automatically by MG/ME.² Since goldstinos appear as the longitudinal modes of massive gravitinos and their interactions become dominant over the transverse modes in high-energy processes, two of the authors also implemented effective goldstino interactions [22] as an alternative to the gravitino code.

In this paper, we revisit the following two processes by using the gravitino implemented MG/ME mentioned above. First, we study associated gravitino productions with a neutralino which promptly decays into a photon and a gravitino in e^+e^- collisions,

$$e^+e^- \rightarrow \tilde{\chi}_1^0 \tilde{G} \rightarrow \gamma \tilde{G} \tilde{G},$$

in the context of a neutralino NLSP with a gravitino LSP. In order to investigate the production cross section and distributions of the photon in detail, we explicitly give the helicity amplitudes for the production process by using the effective goldstino interaction Lagrangian, and present the cross sections with different mass spectra and different energies especially for a future linear collider. We also examine selection efficiencies by kinematical cuts and beam polarizations for the signal and SM background processes, and show that the energy and angular distributions of the photon coming from the neutralino decay can explore the mass of the t -channel exchange selectrons as well as the mass of the decaying neutralino.

Second, we consider gravitino productions in association with a selectron which subsequently decays into an electron and a gravitino at an $e\gamma$ collider, which is an option at a future linear collider [23],

$$e^-\gamma \rightarrow \tilde{e}^- \tilde{G} \rightarrow e^- \tilde{G} \tilde{G},$$

in a slepton co-NLSP scenario with a gravitino LSP. We present the explicit helicity amplitudes for the production process, and discuss the mono-electron plus missing-energy signal, including the Compton back-scattered photon energy spectrum [24, 25] for incident photons. While the heavy-mass limit for all SUSY particles except gravitino and selectron are assumed in Ref. [9], we take into account the t -channel intermediate neutralinos and show a possibility to determine their mass in the signal distributions.

We note in passing that all the helicity amplitudes we present are easily applicable to $q\bar{q} \rightarrow \tilde{g} \tilde{G}$ and to $qg \rightarrow \tilde{q} \tilde{G}$ subprocesses for hadron colliders.

The paper is organized as follows: In Sect. 2 neutralino-gravitino productions in electron-positron collisions are considered, and in Sect. 3 selectron-gravitino productions in electron-photon collisions are studied. Sect. 4 is devoted to our summary. In Appendix A we give the effective goldstino interaction Lagrangian relevant to our study, and in Appendix B we briefly mention neutralino decays into a photon and a gravitino.

2 Neutralino-gravitino production in e^+e^- collisions

In this section, we consider a scenario of a neutralino NLSP with a gravitino LSP, and study associated gravitino productions with a neutralino which promptly decays into a photon and a gravitino in e^+e^- collisions,

$$e^+e^- \rightarrow \tilde{\chi}_1^0 \tilde{G} \rightarrow \gamma \tilde{G} \tilde{G}, \quad (4)$$

leading to a mono-photon plus missing-energy signal.

2.1 Helicity amplitudes

Here we present the helicity amplitudes explicitly for the production process:

$$e^-(p_1, \frac{\lambda_1}{2}) + e^+(p_2, \frac{\lambda_2}{2}) \rightarrow \tilde{\chi}_1^0(p_3, \frac{\lambda_3}{2}) + \tilde{G}(p_4, \frac{\lambda_4}{2}), \quad (5)$$

where the four-momentum (p_i) and helicity ($\lambda_i = \pm 1$) of each particle are defined in the center-of-mass (CM) frame

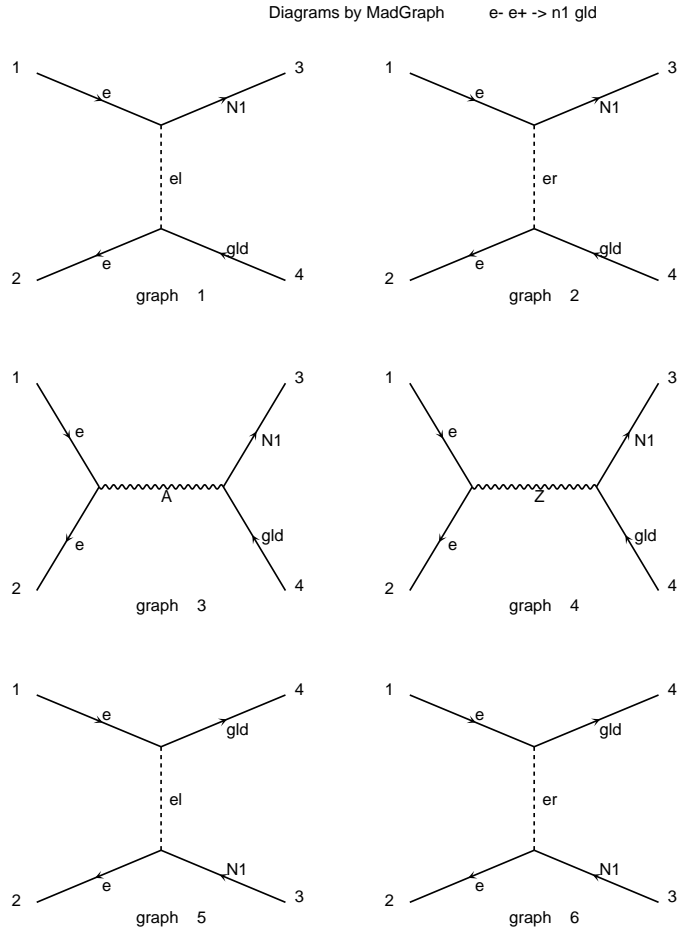


Fig. 1. Feynman diagrams for the $\tilde{\chi}_1^0 \tilde{G}$ production in e^+e^- collisions, generated by MadGraph [22]. N1, gld, el, and er denote a lightest neutralino, a gravitino, a left-handed selectron, and a right-handed selectron, respectively.

² The spin-3/2 functionality is available in MG/ME V4.5 [21].

λ	$\lambda_3\lambda_4$		$\hat{\mathcal{M}}^s$	$\hat{\mathcal{M}}^t$	$\hat{\mathcal{M}}^u$
\pm	$\pm\mp$	$(1 + \cos\theta)$	$\left[\frac{m_{\tilde{\chi}}^2}{s} C_{\pm}^s \right]$		$\left[-\frac{m_{\tilde{\epsilon}}^2}{u-m_{\tilde{\epsilon}}^2} C_{\pm}^{\tilde{\epsilon}\tilde{\chi}1} \right]$
\pm	$\mp\pm$	$-(1 - \cos\theta)$	$\left[\frac{m_{\tilde{\chi}}^2}{s} C_{\pm}^s \right]$	$\left[-\frac{m_{\tilde{\epsilon}}^2}{t-m_{\tilde{\epsilon}}^2} C_{\pm}^{\tilde{\epsilon}\tilde{\chi}1} \right]$	
\pm	$\pm\pm$	$\pm \frac{m_{\tilde{\chi}}}{\sqrt{s}} \sin\theta$	$\left[C_{\pm}^s \right]$	$\left[-\frac{m_{\tilde{\epsilon}}^2}{t-m_{\tilde{\epsilon}}^2} C_{\pm}^{\tilde{\epsilon}\tilde{\chi}1} \right]$	
\pm	$\mp\mp$	$\mp \frac{m_{\tilde{\chi}}}{\sqrt{s}} \sin\theta$	$\left[C_{\pm}^s \right]$		$\left[-\frac{m_{\tilde{\epsilon}}^2}{u-m_{\tilde{\epsilon}}^2} C_{\pm}^{\tilde{\epsilon}\tilde{\chi}1} \right]$

Table 1. The reduced helicity amplitudes $\hat{\mathcal{M}}_{\lambda,\lambda_3\lambda_4}$ for $e_{\lambda}^- e_{-\lambda}^+ \rightarrow \tilde{\chi}_{1\lambda_3}^0 \tilde{G}_{\lambda_4}$.

of the e^+e^- collisions. Throughout our study only the helicity $\pm 1/2$ components of the gravitino, i.e. goldstinos, are considered. In the massless limit of e^{\pm} , one can find that all the amplitudes are zero when both the electron and the positron have the same helicity, or $\lambda_1 = \lambda_2$. In addition, for the $\lambda_1 = +1$ ($\lambda_1 = -1$) case, only the right-handed (left-handed) selectron can contribute to the total amplitudes. Therefore, the helicity amplitudes for the above process can be expressed as the sum of s -, t -, and u -channel amplitudes:

$$\mathcal{M}_{\lambda,\lambda_3\lambda_4} = \mathcal{M}_{\lambda,\lambda_3\lambda_4}^s + \mathcal{M}_{\lambda,\lambda_3\lambda_4}^t + \mathcal{M}_{\lambda,\lambda_3\lambda_4}^u \quad (6)$$

with $\lambda \equiv \lambda_1 = -\lambda_2$, where each amplitude with $\lambda = +1$ ($\lambda = -1$) corresponds to the Feynman graph 3+4, 2 (1), and 6 (5), respectively, in Fig. 1.

We first present the amplitudes based on the effective goldstino interaction Lagrangian, given in Appendix A, in the usual four-spinor basis:

$$i\mathcal{M}_{\lambda,\lambda_3\lambda_4}^s = \frac{e C_{\lambda}^s m_{\tilde{\chi}_1^0}}{2\sqrt{6} \bar{M}_{\text{Pl}} m_{3/2}} \frac{1}{s} \bar{v}(p_2, -\lambda) \gamma^{\mu} u(p_1, \lambda) \times \bar{u}(p_3, \lambda_3) [\not{p}_3 + \not{p}_4, \gamma_{\mu}] v(p_4, \lambda_4), \quad (7a)$$

$$i\mathcal{M}_{\lambda,\lambda_3\lambda_4}^t = \frac{-\sqrt{2} e C_{\lambda}^{\tilde{\epsilon}\tilde{\chi}1} m_{\tilde{\epsilon}_{\lambda}}^2}{\sqrt{3} \bar{M}_{\text{Pl}} m_{3/2}} \frac{1}{t - m_{\tilde{\epsilon}_{\lambda}}^2} \times \bar{u}(p_3, \lambda_3) u(p_1, \lambda) \bar{v}(p_2, -\lambda) v(p_4, \lambda_4), \quad (7b)$$

$$i\mathcal{M}_{\lambda,\lambda_3\lambda_4}^u = \frac{-\sqrt{2} e C_{\lambda}^{\tilde{\epsilon}\tilde{\chi}1} m_{\tilde{\epsilon}_{\lambda}}^2}{\sqrt{3} \bar{M}_{\text{Pl}} m_{3/2}} \frac{1}{u - m_{\tilde{\epsilon}_{\lambda}}^2} \times \bar{u}(p_4, \lambda_4) u(p_1, \lambda) \bar{v}(p_2, -\lambda) v(p_3, \lambda_3), \quad (7c)$$

where $\bar{M}_{\text{Pl}} \equiv M_{\text{Pl}}/\sqrt{8\pi} \sim 2.4 \times 10^{18}$ GeV is the reduced Planck mass, $m_{\tilde{\epsilon}_{\pm}}$ denotes the right-/left-handed selectron mass for notational convenience, and

$$C_{\lambda}^s = C^{\gamma\tilde{\chi}1} - \frac{s}{s - m_Z^2 + i m_Z \Gamma_Z} g_{\lambda} C^{Z\tilde{\chi}1} \quad (8)$$

with Z -boson couplings to right- and left-handed charged leptons,

$$g_{+} = \frac{\sin\theta_W}{\cos\theta_W} \quad \text{and} \quad g_{-} = \frac{-1 + 2\sin^2\theta_W}{2\sin\theta_W \cos\theta_W}, \quad (9)$$

respectively.³ The couplings related to the neutralino mixing defined by $X_i = U_{ij} \tilde{\chi}_j^0$ in the $X = (\tilde{B}, \tilde{W}^3, \tilde{H}_d^0, \tilde{H}_u^0)$ basis, where U_{ij} is taken to be real, are

$$\begin{aligned} C^{\gamma\tilde{\chi}i} &= U_{1i} \cos\theta_W + U_{2i} \sin\theta_W, \\ C^{Z\tilde{\chi}i} &= -U_{1i} \sin\theta_W + U_{2i} \cos\theta_W, \\ C_{\pm}^{\tilde{\epsilon}\tilde{\chi}i} &= T_{\pm}^{\tilde{\epsilon}} \frac{U_{2i}}{\sin\theta_W} + Y_{\pm}^{\tilde{\epsilon}} \frac{U_{1i}}{\cos\theta_W}, \end{aligned} \quad (10)$$

with the $SU(2)$ charge $T_{\pm}^{\tilde{\epsilon}}$ and the $U(1)$ charge $Y_{\pm}^{\tilde{\epsilon}}$ for $\tilde{e}_{\pm} (= \tilde{e}_{R/L})$. Here, for simplicity, we assume the lightest neutralino as a pure gaugino, which makes the \tilde{G} - $\tilde{H}_{d,u}^0$ - Z couplings irrelevant to our study. It should be noted that C_{λ}^s and $C_{\lambda}^{\tilde{\epsilon}\tilde{\chi}1}$ are related with each other as

$$C_{\lambda}^s \sim -C_{\lambda}^{\tilde{\epsilon}\tilde{\chi}1} + \mathcal{O}\left(\frac{m_Z^2}{s}\right) \quad (11)$$

for $\sqrt{s} \gg m_Z$; this is always the case in the following discussions.

To present the explicit helicity amplitudes, let us now define the kinematical variables of the process (5) in the e^+e^- laboratory frame as

$$\begin{aligned} p_1^{\mu} &= \frac{\sqrt{s}}{2} (1, 0, 0, 1), \\ p_2^{\mu} &= \frac{\sqrt{s}}{2} (1, 0, 0, -1), \\ p_3^{\mu} &= \frac{\sqrt{s}}{2} \left(1 + \frac{m_{\tilde{\chi}}^2}{s}, \beta \sin\theta, 0, \beta \cos\theta\right), \\ p_4^{\mu} &= \frac{\sqrt{s}}{2} \left(1 - \frac{m_{\tilde{\chi}}^2}{s}, -\beta \sin\theta, 0, -\beta \cos\theta\right), \end{aligned} \quad (12)$$

with $\beta = 1 - m_{\tilde{\chi}_1^0}^2/s$. Throughout our study we neglect the gravitino mass, except in the gravitino couplings.

For notational convenience we define the reduced helicity amplitudes, $\hat{\mathcal{M}}$, as

$$i\mathcal{M}_{\lambda,\lambda_3\lambda_4} = \frac{-e}{\sqrt{6} \bar{M}_{\text{Pl}} m_{3/2}} \sqrt{\beta} s \hat{\mathcal{M}}_{\lambda,\lambda_3\lambda_4}, \quad (13)$$

and these are presented in Table 1. The following features of the amplitudes are worth noting:

³ Strictly speaking, the Z -exchange amplitude in (7a) is valid only for $\sqrt{s} \gg m_Z$ since massless gauge bosons are assumed in the effective Lagrangian (38).

1. As mentioned before, for the $\lambda = +1$ ($\lambda = -1$) case only \tilde{e}_+ (\tilde{e}_-) can be exchanged in the t - and u -channel amplitudes, and all the amplitudes are zero for $\lambda_1 = \lambda_2$.
2. The overall angular dependence is dictated by $J = 1$ d functions as

$$\mathcal{M}_{\lambda, \lambda_3 \lambda_4} \propto d_{\lambda, (\lambda_3 - \lambda_4)/2}^1(\theta). \quad (14)$$

3. \mathcal{M}^s and $\mathcal{M}^{t,u}$ interfere subtractively with each other; especially for the $\lambda_3 = \lambda_4$ case they almost cancel in the wide range of the parameter space, and hence the amplitudes with $\lambda_3 = -\lambda_4$ are dominant for the most of the cases except for the $m_{\tilde{\chi}_1^0} \sim m_{\tilde{e}_\pm}$ region. We note that in the very high-energy region the amplitudes with $\lambda_3 = \lambda_4$ become important since \mathcal{M}^s becomes dominant, making those amplitudes be proportional to \sqrt{s} while the amplitudes with $\lambda_3 = -\lambda_4$ are independent of \sqrt{s} ; in that region the cross section does not depend on the selectron masses but on the produced neutralino mass.
4. For the $\lambda_3 = -\lambda_4$ case, in the threshold region, where $t, u = -s\beta(1 \mp \cos\theta)/2 \rightarrow 0$, an additional β can be extracted from the reduced amplitudes due to $C_\pm^s \sim -C_\pm^{\tilde{e}\tilde{\chi}_1}$ in (11). Together with $\beta^{1/2}$ in (13), the amplitudes are proportional to $\beta^{3/2}$. Therefore, including the phase space factor β , the threshold excitation of the total cross section is given by [5, 7, 8]⁴

$$\sigma \propto \beta^4. \quad (15)$$

5. \mathcal{M}^t and \mathcal{M}^u depend on the selectron mass and become larger as the selectron mass increases, while \mathcal{M}^s is independent of $m_{\tilde{e}}$.

We note that our helicity-summed amplitude squared agrees with Eq. (28) in [8] for the photino case, and also with Eq. (3) of [12] for the gluino associated process $q\bar{q} \rightarrow \tilde{g}\tilde{G}$ after substitutions for the masses and the couplings as

$$\begin{aligned} m_{\tilde{\chi}_1^0} &\rightarrow m_{\tilde{g}}, & m_{\tilde{e}_{R/L}} &\rightarrow m_{\tilde{q}_{R/L}}, \\ e &\rightarrow -g_s T^a, & C_\lambda^s &\rightarrow 1, & C_\lambda^{\tilde{e}\tilde{\chi}_1} &\rightarrow -1. \end{aligned} \quad (16)$$

Moreover, our analytic amplitudes are checked numerically for each helicity combination by using the gravitino/goldstino code in MG/ME [17, 22].

2.2 Cross sections and kinematical distributions

Let us now present the total cross sections and the kinematical distributions for the production process (5). The initial-helicity (λ) dependent cross section is given by

$$d\sigma_\lambda = \frac{1}{2s} \frac{1}{2} \sum_{\lambda_{3,4}} |\mathcal{M}_{\lambda, \lambda_3 \lambda_4}|^2 d\Phi_2 \quad (17)$$

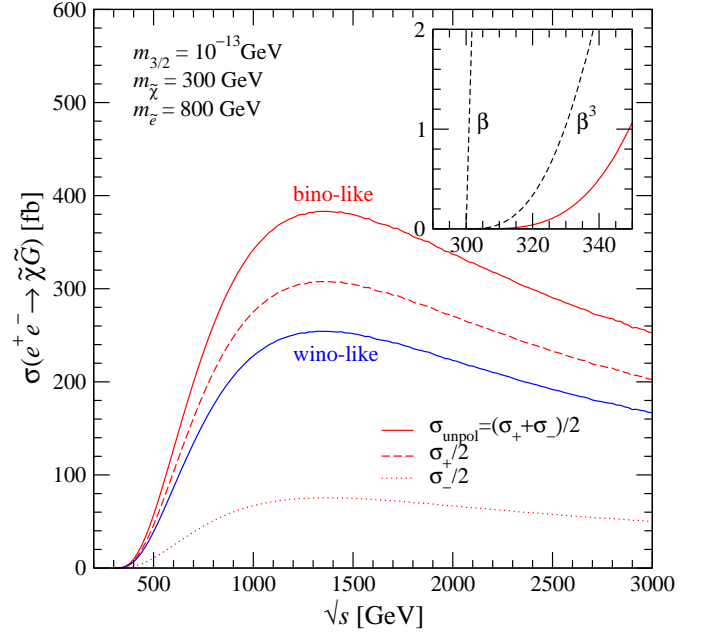


Fig. 2. Total cross sections of associated gravitino productions with a bino-/wino-like neutralino in e^+e^- collisions, $e^+e^- \rightarrow \tilde{\chi}_1^0 \tilde{G}$, for $m_{3/2} = 10^{-13}$ GeV as a function of the collision energy. The neutralino and selectron masses are fixed at 300 GeV and 800 GeV, respectively. The initial-helicity dependent cross sections σ_λ are shown by a dashed line for $\lambda = +1$ and a dotted line for $\lambda = -1$. The threshold region is enlarged and the hypothetical dependence $\sigma \propto \beta$ and β^3 with the same coefficient is also shown.

with the two-body phase space factor $d\Phi_2$. $\sigma_{\text{unpol}} = (\sigma_+ + \sigma_-)/2$ is the usual spin-summed and averaged cross section.

Figure 2 shows total cross sections of the gravitino productions associated with a bino-/wino-like neutralino in e^+e^- collisions as a function of the CM energy \sqrt{s} , where the neutralino and selectron masses are fixed as $m_{\tilde{\chi}_1^0} = 300$ GeV and $m_{\tilde{e}_+} = m_{\tilde{e}_-} = 800$ GeV. It should be stressed that the cross section scales with $m_{3/2}^{-2}$, and we fix the gravitino mass $m_{3/2} = 10^{-13}$ GeV in our study so that the production cross sections are around $\mathcal{O}(10^1 \sim 10^3)$ fb. In the figure the threshold region for the unpolarized bino-like neutralino cross section is enlarged, and one can see that the production cross section is strongly suppressed as shown in (15), in contrast to the threshold excitation for the standard fermion ($\propto \beta$) and the scalar ($\propto \beta^3$) pair productions [26]. This is one of the particular signatures for the associated gravitino productions.

For the case of the bino-like neutralino, or $|U_{11}| \sim 1$ and $|U_{21}| \sim 0$ in (10), the cross section with right-handed electrons (σ_+) dominates the one with left-handed (σ_-). For the heavy selectron case the t - and u -channel contributions are dominant, and therefore the ratio of the λ -dependent cross sections is roughly given in terms of the

⁴ Note that β is defined as $(1 - m_{\tilde{\chi}_1^0}^2/s)^{1/2}$ in Refs. [7, 8].

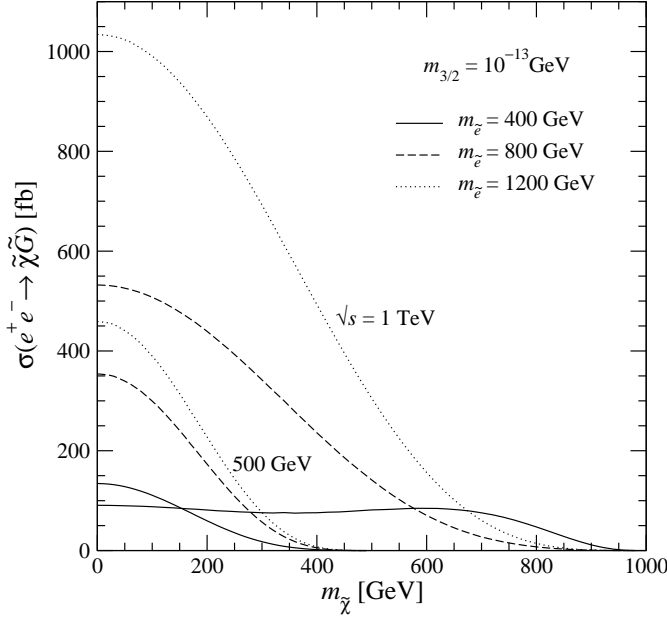


Fig. 3. Total cross sections of $e^+e^- \rightarrow \tilde{\chi}_1^0 \tilde{G}$ at $\sqrt{s} = 500$ GeV and 1 TeV for $m_{3/2} = 10^{-13}$ GeV as a function of the neutralino mass. The selectron masses are fixed at 400 (solid), 800 (dashed) and 1200 (dotted) GeV, respectively.

$\tilde{\chi}_1^0$ - e - \tilde{e}_\pm couplings as

$$\frac{\sigma_\pm}{2\sigma_{\text{unpol}}} \sim \frac{|C_\pm^{\tilde{e}\tilde{\chi}_1}|^2}{|C_+^{\tilde{e}\tilde{\chi}_1}|^2 + |C_-^{\tilde{e}\tilde{\chi}_1}|^2}. \quad (18)$$

The bino case gives $\sigma_+/2\sigma_{\text{unpol}} \sim 0.8$, which one can observe in Fig. 2. On the other hand, for the case of the wino-like neutralino, or $|U_{11}| \sim 0$ and $|U_{21}| \sim 1$, the right-handed cross section vanishes, i.e. $\sigma_{\text{unpol}} = \sigma_-/2$. One can conclude that the $\tilde{\chi}_1^0$ - \tilde{G} production process with polarized electron beam can explore the neutralino mixing. The detailed study for various neutralino mixing has been done in Refs. [7,8], while we assume a bino-like neutralino in the following analyses for simplicity, which is often the case in GMSB; see, e.g. Fig. 4 in [27].

In Fig. 3, the neutralino-mass dependence of the cross sections is shown for $\sqrt{s} = 500$ GeV and 1 TeV. Due to the threshold behavior in (15), the cross sections are strongly suppressed as the neutralino mass is approaching the collider energy.⁵ It should be emphasized here that the cross section is quite sensitive to the mass of the t, u -channel intermediate selectrons, even if the collider energy cannot reach them [7,8]. The heavier selectron exchange increases the cross section since the t, u -channel amplitudes are proportional to the selectron mass squared as one can see in Table 1. We also note that, however, the goldstino couplings become too strong at some point for heavy selectrons to perform the reliable perturbative calculations.

⁵ For the case of $m_{\tilde{e}_\pm} = 400$ GeV at $\sqrt{s} = 1$ TeV, the cross section is not so strongly suppressed as β^4 . This is because in this parameter region the contributions from the amplitudes with $\lambda_3 = \lambda_4$ are significant and these amplitudes do not provide an additional suppression factor β .

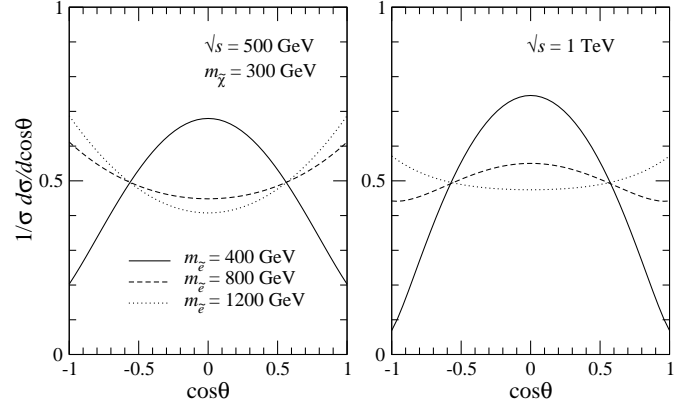


Fig. 4. Normalized angular distributions of the neutralino in $e^+e^- \rightarrow \tilde{\chi}_1^0 \tilde{G}$ at $\sqrt{s} = 500$ GeV (left) and 1 TeV (right) for $m_{\tilde{\chi}_1^0} = 300$ GeV, where the selectron masses are taken to be 400, 800 and 1200 GeV.

Before taking the neutralino decay into account, we discuss the angular distribution of the produced neutralino since the $\tilde{\chi}_1^0 \rightarrow \gamma \tilde{G}$ decay is isotropic (see Appendix B) and hence the photon distribution is given by purely kinematical effects of the decaying neutralino. In Fig. 4, the normalized $\cos \theta$ distributions of the neutralino in $e^+e^- \rightarrow \tilde{\chi}_1^0 \tilde{G}$ at $\sqrt{s} = 500$ GeV (left) and 1 TeV (right) are shown for $m_{\tilde{\chi}_1^0} = 300$ GeV. One can find that not only the total cross section as shown in Fig. 3 but also the angular distribution is quite sensitive to the mass of the t, u -channel intermediate selectrons [8]. When the selectron mass is close to the neutralino mass, the cross section is suppressed around $|\cos \theta| = 1$ since a cancellation occurs between \mathcal{M}^s and $\mathcal{M}^{t,u}$ for the $\lambda_3 = -\lambda_4$ case due to $(t - m_{\tilde{e}}^2) = -s$ for $\cos \theta = -1$ and $(u - m_{\tilde{e}}^2) = -s$ for $\cos \theta = 1$; see also Table 1. For the heavy selectron case, on the other hand, the neutralino tends to be produced to the forward and backward regions since the selectron exchange diagrams are dominant and give the $(1 + \cos \theta)^2$ or $(1 - \cos \theta)^2$ angular dependence. We note that the contributions from the $\lambda_3 = \lambda_4$ case, which could give $\sin^2 \theta$ dependence, are negligible for heavy selectron masses as mentioned before.

Let us now turn to the simulation for the single-photon signal with missing energy. The partial decay rate of the neutralino decay into a photon and a gravitino is given by (see also Appendix B)

$$\Gamma(\tilde{\chi}_1^0 \rightarrow \gamma \tilde{G}) = \frac{|C^{\gamma \tilde{\chi}_1}|^2 m_{\tilde{\chi}_1^0}^5}{48\pi \overline{M}_{\text{Pl}}^2 m_{3/2}^2}, \quad (19)$$

and $\Gamma(\tilde{\chi}_1^0 \rightarrow \gamma \tilde{G}) = 0.21$ GeV for the bino-like neutralino with $m_{\tilde{\chi}_1^0} = 300$ GeV and $m_{3/2} = 10^{-13}$ GeV. An irreducible SM background for the signal of mono-photon plus missing energy comes from $e^+e^- \rightarrow \gamma \nu \bar{\nu}$. In addition to the minimal cuts for the detection of photons

$$E_\gamma > 0.03 \sqrt{s}, \quad |\eta_\gamma| < 2, \quad (20)$$

σ [fb]		$(P_{e^-}, P_{e^+}) =$	(0, 0)	(0.9, 0)	(0.9, -0.6)
$\sqrt{s} = 500$ GeV	$m_{\tilde{e}} = 400$ GeV		15	23	37
	800 GeV		48	75	119
	1200 GeV		64	100	159
	SM background		1592	178	94
$\sqrt{s} = 1$ TeV	$m_{\tilde{e}} = 400$ GeV		72	112	177
	800 GeV		320	494	785
	1200 GeV		642	1002	1582
	SM background		1443	149	65

Table 2. Cross sections in fb unit for the signal, $e^+e^- \rightarrow \tilde{\chi}_1^0 \tilde{G} \rightarrow \gamma \tilde{G} \tilde{G}$, and the SM background, $e^+e^- \rightarrow \gamma \nu \bar{\nu}$, at $\sqrt{s} = 500$ GeV and 1 TeV with different beam polarizations P_{e^\pm} . We take $m_{3/2} = 10^{-13}$ GeV, $m_{\tilde{\chi}_1^0} = 300$ GeV, and $B(\tilde{\chi}_1^0 \rightarrow \gamma \tilde{G}) = 1$. The minimal cuts in (20) and the Z-peak cut in (21) are taken into account.

we impose the Z-peak cut

$$E_\gamma < \frac{s - m_Z^2}{2\sqrt{s}} - 5\Gamma_Z, \quad (21)$$

which can remove the contributions from $e^+e^- \rightarrow \gamma Z \rightarrow \gamma \nu \bar{\nu}$. The most significant background coming from the t -channel W -exchange process can be reduced by using polarized e^\pm beams.

In Table 2, the selection efficiencies for the signal and background processes with different polarizations⁶ are presented, where the above kinematical cuts, (20) and (21), are taken into account. The cross sections both for the signal and background are calculated by MG/MEv4 [21] supporting gravitino interactions [17, 22]. Here, we assume the branching ratio of the neutralino decay is unity, $B(\tilde{\chi}_1^0 \rightarrow \gamma \tilde{G}) = 1$, although other decay modes can be significant in some parameter space [27]. Since the cross section with e^\pm beam polarizations P_{e^\pm} ($|P_{e^\pm}| \leq 1$) is given by

$$\sigma(P_{e^-}, P_{e^+}) = 2 \sum_\lambda \left(\frac{1 + P_{e^-} \lambda}{2} \right) \left(\frac{1 - P_{e^+} \lambda}{2} \right) \sigma_\lambda, \quad (22)$$

the signal cross section for the bino-like neutralino can be enhanced, while the background can be reduced quite effectively, by using a positively polarized e^- beam ($P_{e^-} > 0$) and a negatively polarized e^+ beam ($P_{e^+} < 0$). It must be noted again that the signal cross section is inversely proportional to the gravitino mass squared.

Figure 5 shows normalized energy distributions of the photon for the signal and the SM background, corresponding to 20,000 events each, at $\sqrt{s} = 500$ GeV (left) and 1 TeV (right), where the selectron mass of 400, 800 and 1200 GeV with the 300 GeV neutralino mass are considered. The kinematical cuts in (20) and (21) and the beam polarizations $(P_{e^-}, P_{e^+}) = (0.9, -0.6)$ are taken into account. The signal distributions are flat, independent of the selectron mass,⁷ and restricted as

$$\frac{m_{\tilde{\chi}_1^0}^2}{2\sqrt{s}} < E_\gamma < \frac{\sqrt{s}}{2}, \quad (23)$$

⁶ $|P_{e^-}| > 0.8$ and $|P_{e^+}| > 0.5$ are designed at the International Linear Collider (ILC) [23].

⁷ We point out that the photonic energy distributions of Fig. 5 in Ref. [8] should be flat and not depend on the selectron mass.

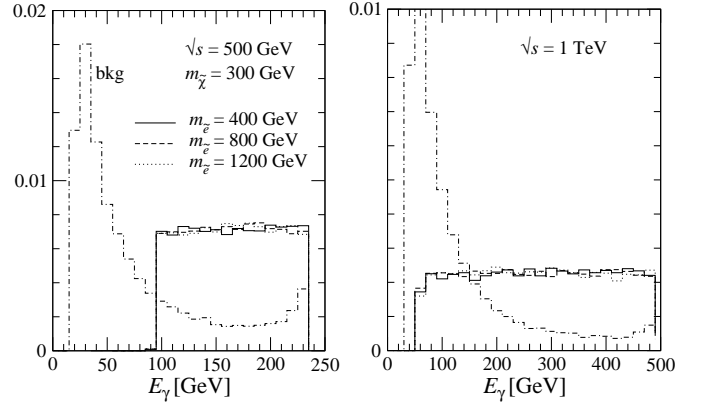


Fig. 5. Normalized energy distributions of the photon for $e^+e^- \rightarrow \tilde{\chi}_1^0 \tilde{G} \rightarrow \gamma \tilde{G} \tilde{G}$ at $\sqrt{s} = 500$ GeV (left) and 1 TeV (right), where $m_{\tilde{e}^\pm} = 400$ (solid), 800 (dashed) and 1200 (dotted) GeV with $m_{\tilde{\chi}_1^0} = 300$ GeV are considered. The kinematical cuts in (20) and (21) and the beam polarizations $(P_{e^-}, P_{e^+}) = (0.9, -0.6)$ are taken into account. Those of the SM background are also shown by dot-dashed lines.

where the lower edge can determine the mass of the neutralino. It should be stressed again that the photon distribution is simply given by kinematical effects of the decaying neutralino. The background is mostly distributed in the low-energy region, and hence a further cut on the photon energy would be useful to enhance the signal over background.

Finally, we present the angular dependence of the photon in the laboratory frame in Fig. 6. The original angular distributions of the neutralino in Fig. 4 are flattened for the case of a 500 GeV collider since the neutralino decays isotropically in its rest frame and the boost effect is small. On the other hand, the angular distributions still survive for the case of a 1 TeV collider. This indicates a possibility to examine the mass of the t, u -channel selectrons when the decaying neutralino has a large momentum. We note that a kinematical cut on the forward and backward regions would also help to reduce the background.

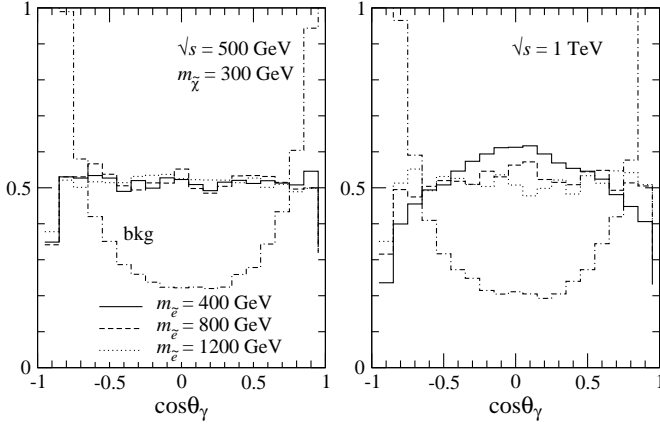


Fig. 6. Normalized angular distributions of the photon in the laboratory frame for $e^+e^- \rightarrow \tilde{\chi}_1^0 \tilde{G} \rightarrow \gamma \tilde{G} \tilde{G}$. The detail is the same as Fig. 5.

3 Selectron-gravitino production in $e^-\gamma$ collisions

In this section, we repeat a study as in Sect. 2 for a scenario of a selectron NLSP with a gravitino LSP. We consider associated gravitino productions with a selectron, especially a right-handed selectron, in $e^-\gamma$ collisions with the prompt selectron decay into an electron and a gravitino,

$$e^-\gamma \rightarrow \tilde{e}_R \tilde{G} \rightarrow e^- \tilde{G} \tilde{G}, \quad (24)$$

leading to a mono-electron plus missing-energy signal.

3.1 Helicity amplitudes

Here we present the helicity amplitudes explicitly for the production process:

$$e^-\left(p_1, \frac{\lambda_1}{2}\right) + \gamma(p_2, \lambda_2) \rightarrow \tilde{e}_R^-(p_3) + \tilde{G}\left(p_4, \frac{\lambda_4}{2}\right). \quad (25)$$

The helicity amplitudes for the process are expressed as sums of s -, t -, and u -channel amplitudes

$$\mathcal{M}_{\lambda_1 \lambda_2 \lambda_4} = \mathcal{M}^s + \sum_{i=1}^4 \mathcal{M}^{t_i} + \mathcal{M}^u, \quad (26)$$

corresponding to the Feynman graph 6, (2+3+4+5), and 1, respectively, in Fig. 7. They are given in the four-spinor

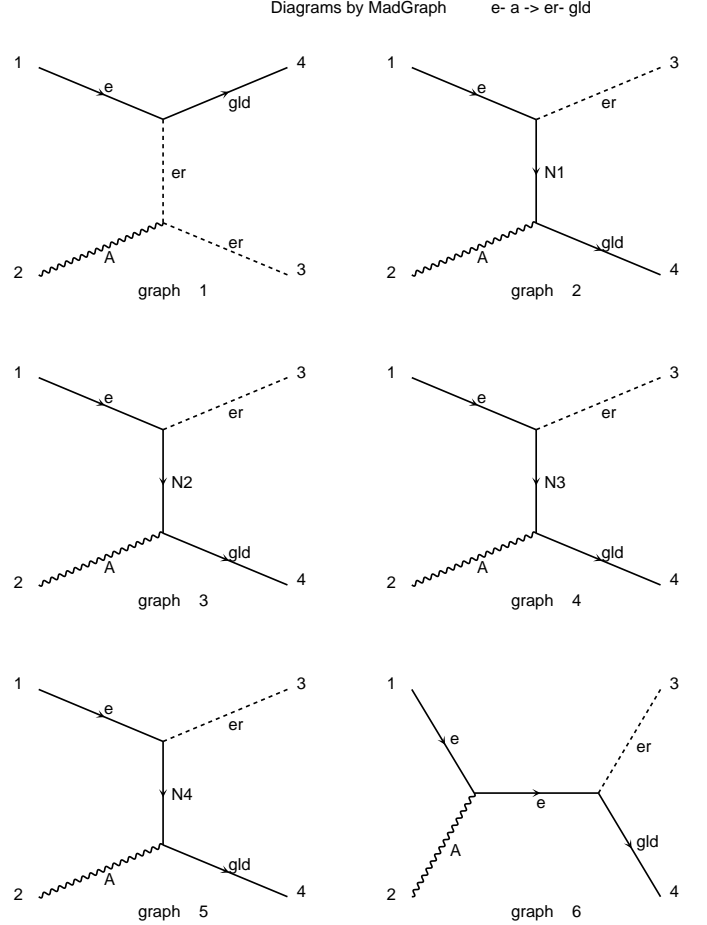


Fig. 7. Feynman diagrams for the $\tilde{e}_R^- \tilde{G}$ production in $e^-\gamma$ collisions, generated by MadGraph [22].

basis by

$$i\mathcal{M}_{\lambda_1 \lambda_2 \lambda_4}^s = \frac{-e m_{\tilde{e}_{\lambda_1}}^2}{\sqrt{3} \bar{M}_{\text{Pl}} m_{3/2}} \frac{1}{s} \epsilon_\mu(p_2, \lambda_2) \times \bar{u}(p_4, \lambda_4) (\not{p}_1 + \not{p}_2) \gamma^\mu u(p_1, \lambda_1), \quad (27a)$$

$$i\mathcal{M}_{\lambda_1 \lambda_2 \lambda_4}^{t_i} = \frac{e m_{\tilde{\chi}_i^0} C^{\gamma \tilde{\chi}_i} C_{\lambda_1}^{\tilde{e} \tilde{\chi}_i}}{2\sqrt{3} \bar{M}_{\text{Pl}} m_{3/2}} \frac{1}{t - m_{\tilde{\chi}_i^0}^2} \epsilon_\mu(p_2, \lambda_2) \times \bar{u}(p_4, \lambda_4) [\not{p}_2, \gamma^\mu] (\not{p}_1 - \not{p}_3 + m_{\tilde{\chi}_i^0}) u(p_1, \lambda_1), \quad (27b)$$

$$i\mathcal{M}_{\lambda_1 \lambda_2 \lambda_4}^u = \frac{-e m_{\tilde{e}_{\lambda_1}}^2}{\sqrt{3} \bar{M}_{\text{Pl}} m_{3/2}} \frac{1}{u - m_{\tilde{e}_{\lambda_1}}^2} \epsilon_\mu(p_2, \lambda_2) \times \bar{u}(p_4, \lambda_4) u(p_1, \lambda_1) (p_3 + p_1 - p_4)^\mu, \quad (27c)$$

with the couplings $C^{\gamma \tilde{\chi}_i}$ and $C_{\pm}^{\tilde{e} \tilde{\chi}_i}$ defined in (10). Only the $\lambda_1 = +1$ case contributes to the \tilde{e}_R (or \tilde{e}_+ in our notation) production in the final state, which is relevant in our following analyses. On the other hand, the $\lambda_1 = -1$ case gives nonzero amplitudes only for the \tilde{e}_L production.

$\lambda_1 \lambda_2$	λ_4	$\hat{\mathcal{M}}^s$	$\hat{\mathcal{M}}^t$	$\hat{\mathcal{M}}^u$
++	-	$2 \sin \frac{\theta}{2}$	$\left[\frac{m_{\tilde{e}}^2}{s} - \sum_i C^{\gamma \tilde{\chi}_i} C_{+}^{\tilde{e} \tilde{\chi}_i} \frac{m_{\tilde{\chi}_i}^2}{t - m_{\tilde{\chi}_i}^2} + \frac{m_{\tilde{e}}^2}{u - m_{\tilde{e}}^2} \beta \frac{1 + \cos \theta}{2} \right]$	
+-	+	$(1 - \cos \theta) \cos \frac{\theta}{2}$	$\left[- \sum_i C^{\gamma \tilde{\chi}_i} C_{+}^{\tilde{e} \tilde{\chi}_i} \frac{\sqrt{s} m_{\tilde{\chi}_i}}{t - m_{\tilde{\chi}_i}^2} \beta \right]$	
+-	-	$-(1 + \cos \theta) \sin \frac{\theta}{2}$		$\left[\frac{m_{\tilde{e}}^2}{u - m_{\tilde{e}}^2} \beta \right]$

Table 3. The reduced helicity amplitudes $\hat{\mathcal{M}}_{\lambda_1 \lambda_2, \lambda_4}$ for $e_{\lambda_1}^- \gamma_{\lambda_2} \rightarrow \tilde{e}_{\lambda_4}^- \tilde{G}_{\lambda_4}$.

We define the reduced helicity amplitudes, $\hat{\mathcal{M}}$, as

$$i\mathcal{M}_{\lambda_1 \lambda_2, \lambda_4} = \frac{-e}{\sqrt{6} \bar{M}_{\text{Pl}} m_{3/2}} \sqrt{\beta} s \hat{\mathcal{M}}_{\lambda_1 \lambda_2, \lambda_4}, \quad (28)$$

and these are shown in Table 3. Similar to (12), the four-momenta and helicities of the external particles are defined in the $e\gamma$ CM frame with $\beta = 1 - m_{\tilde{e}_R}^2/s$. The following features of the amplitudes are worth noting:

1. The amplitude $\mathcal{M}_{+,+,+}$ is zero since the coupling structures do not allow this helicity combination for a massless goldstino.
2. The overall angular dependence is dictated by $J = 1/2$ or $J = 1$ d functions as

$$\mathcal{M}_{\lambda_1 \lambda_2, \lambda_4} \propto d_{\lambda_1/2 - \lambda_2, -\lambda_4/2}^{|\lambda_1/2 - \lambda_2|}(\theta). \quad (29)$$

3. The amplitude \mathcal{M}^t depends on the mass of the propagating neutralinos; as the neutralino mass increases, $\mathcal{M}_{+,+,-}^t$ becomes larger, while $\mathcal{M}_{+,-,+}^t$ becomes smaller. On the other hand, the \mathcal{M}^s and \mathcal{M}^u do not depend on their mass but on the selectron mass.
4. The right-handed selectron can couple only to the bino component of neutralinos $\tilde{\chi}_i^0$, i.e. U_{1i} in the $\tilde{\chi}_i^0 - e - \tilde{e}_R$ coupling in (10). Therefore, e.g. for the bino-like lightest neutralino case, only the $\tilde{\chi}_1^0$ -exchange amplitude is nonzero among the four neutralino amplitudes.
5. In the threshold region, similar to the $e^+e^- \rightarrow \tilde{\chi}_1^0 \tilde{G}$ process, the amplitudes are proportional to $\beta^{3/2}$, which gives rise to the strong suppression on the production cross section.
6. In the high-energy limit, the amplitude $\mathcal{M}_{+,-,+}$ becomes dominant, and hence the cross section depends on the neutralino mass but not on the produced selectron mass.

We note that our helicity amplitudes in Table 3 agree with Eqs. (4) and (5) in [9],⁸ where the heavy neutralino mass limit is assumed. The helicity-summed amplitude squared also agrees with Eq. (7) of [12] for the squark associated process $q\bar{q} \rightarrow \tilde{q} \tilde{G}$ after substitutions for the masses and the couplings as in (16) and the exchange of $t \leftrightarrow u$. Moreover, we checked our amplitudes for each helicity combination numerically by the gravitino/goldstino code in MG/ME [17, 22].

⁸ Except the sign in the parentheses of the first term in Eq. (4) in [9].

3.2 Cross sections and kinematical distributions

In practice, a high-energy photon beam is provided by the backward Compton scattering of laser photons on a high-energy electron beam [24, 25], as an option of a future linear collider [23]. Let us introduce the photon luminosity function [24, 28]

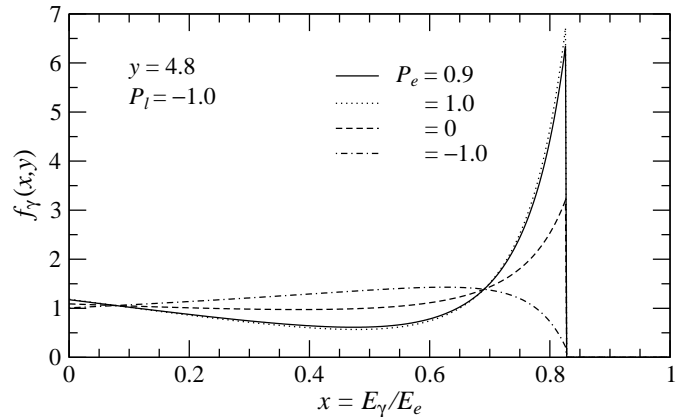
$$f_\gamma(x, y) = \frac{1}{N(y)} \left[\frac{1}{1-x} + 1 - x - 4r(1-r) + P_e P_l r y (1-2r)(2-x) \right], \quad (30)$$

where $x = E_\gamma/E_e$ is the energy ratio of the scattered photon and the electron beam, y is a parameter controlled by the laser energy,⁹ $r = x/(1-x)y$, and P_e (P_l) is the incident electron beam (laser photon) polarization. The integral $\int f_\gamma(x, y) dx$ is normalized to unity by

$$N(y) = \left(1 - \frac{4}{y} - \frac{8}{y^2} \right) \ln(1+y) + \frac{1}{2} + \frac{8}{y} - \frac{1}{2(1+y)^2} + P_e P_l \left[\left(1 + \frac{2}{y} \right) \ln(1+y) - \frac{5}{2} + \frac{1}{1+y} - \frac{1}{2(1+y)^2} \right]. \quad (31)$$

Figure 8 shows the luminosity function for different electron beam polarizations, with $y = 4.8$ and $P_l = -1.0$ as an optimal parameter choice [28]. The maximal energy fraction is fixed by $x_{\text{max}} = y/(1+y)$, e.g. $x_{\text{max}} \sim 0.83$ for

⁹ $y = 4E_e E_l / m_e^2$ in the zero angle limit of the Compton scattering.

**Fig. 8.** The distribution functions of Compton back-scattered photons in (30) for different electron beam polarizations.

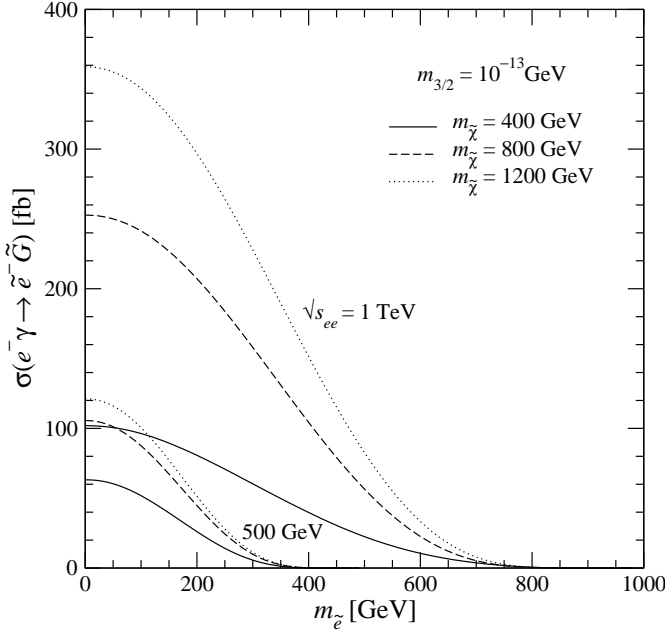


Fig. 9. Total cross sections of associated gravitino productions with a right-handed selectron in $e^-\gamma$ collisions, $e^-\gamma \rightarrow \tilde{e}_R^-\tilde{G}$, at $\sqrt{s_{ee}} = 500$ GeV and 1 TeV for $m_{3/2} = 10^{-13}$ GeV as a function of the selectron mass. The neutralino mass is fixed at 400 (solid), 800 (dashed) and 1200 (dotted) GeV, respectively.

$y = 4.8$. The distribution with highly polarized electron and laser beams ($P_e P_l \sim -1$) has a strong peak at the high-energy endpoint.¹⁰

The full cross section at an $e\gamma$ collider is calculated by convoluting the $e\gamma$ cross section ($\sigma^{e\gamma}$) with the photon distribution function of Eq. (30) as

$$\sigma(s_{ee}) = \int_{x_{\min}}^{x_{\max}} f_\gamma(x, y) \sigma^{e\gamma}(s) dx \quad (32)$$

with $x_{\min} = m_{\tilde{e}}^2/s_{ee}$ and $s = xs_{ee}$, where $\sqrt{s_{ee}}$ is the original e^-e^- CM energy. The spin-summed and averaged $e\gamma$ cross section is obtained by $\sigma^{e\gamma} = (\sigma_+^{e\gamma} + \sigma_-^{e\gamma})/2$ with the photon-helicity (λ_2) dependent cross section

$$d\sigma_{\lambda_2}^{e\gamma} = \frac{1}{2s} \frac{1}{2} \sum_{\lambda_1, \lambda_4} |\mathcal{M}_{\lambda_1 \lambda_2, \lambda_4}|^2 d\Phi_2. \quad (33)$$

Figure 9 shows total cross sections of the associated gravitino productions with a right-handed selectron in $e^-\gamma$ collisions as a function of the selectron mass, where the CM energy, $\sqrt{s_{ee}}$, of the e^-e^- system is fixed at 500 GeV and 1 TeV. The parameters for the photon luminosity function in (30) are taken to be $y = 4.8$ and $P_e P_l = -0.9$. For simplicity, we assume a bino-like lightest neutralino so that only the $\tilde{\chi}_1^0$ -exchange amplitude is taken into account

¹⁰ Although the scattered photons are polarized when $P_e \neq 0$ or $P_l \neq 0$ [25, 28], we average the two opposite polarized modes, ($P_e > 0, P_l < 0$) and ($P_e < 0, P_l > 0$), so that we consider $f_\gamma(x, y)$ as the unpolarized distribution function in the following analyses.

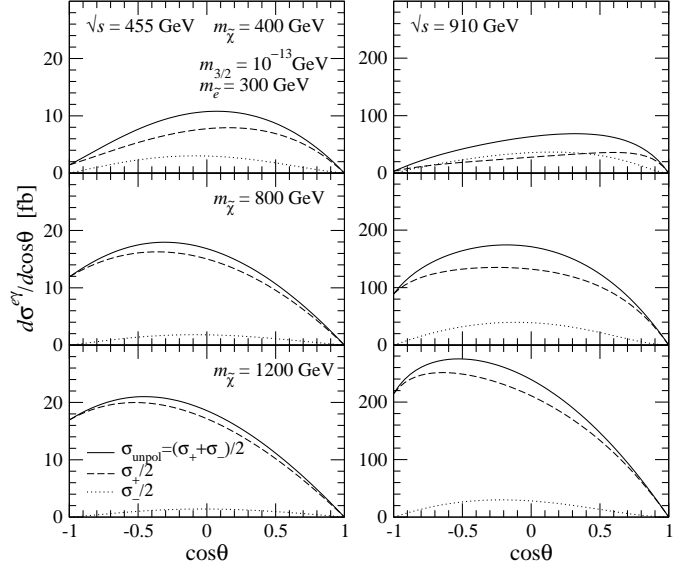


Fig. 10. Angular distributions of the selectron in $e^-\gamma \rightarrow \tilde{e}_R^-\tilde{G}$ at $\sqrt{s} = 455$ (left) and 910 (right) GeV in the $e\gamma$ CM frame, with $m_{3/2} = 10^{-13}$ GeV and $m_{\tilde{e}_R} = 300$ GeV. The neutralino mass is taken to be 400 (top), 800 (middle) and 1200 (bottom) GeV, respectively. The photon-helicity dependent cross sections $d\sigma_{\lambda_2}^{e\gamma}$ are also shown by dashed lines ($\lambda_2 = +1$) and dotted lines ($\lambda_2 = -1$).

for the t -channel amplitude; see comment 4 in Sect. 3.1. We note that $\sigma \propto 1/m_{3/2}^2$ and we take $m_{3/2} = 10^{-13}$ GeV in our study. When the selectron mass is close to the collider energy, the cross sections are strongly suppressed due to $\sigma^{e\gamma} \propto \beta^4$ as mentioned in comment 5 in Sect. 3.1, similar to the $e^+e^- \rightarrow \tilde{\chi}_1^0 \tilde{G}$ process in Fig. 3. In addition, the production cross section is nonzero only when $m_{\tilde{e}_R} < \sqrt{x_{\max} s_{ee}}$. It should be stressed here that the cross section is quite sensitive to the mass of the t -channel intermediate neutralinos, even if the collider energy cannot reach their mass.

Before we consider the selectron decay, let us look in detail at the angular distribution of the produced selectron in the $e\gamma$ system since the scalar decay $\tilde{e}_R \rightarrow e\tilde{G}$ is isotropic and hence the electron distribution is given by purely kinematical effects of the decaying selectron and the boost from the $e^-\gamma$ CM frame to the e^-e^- laboratory frame. In Fig. 10, the $\cos\theta$ distributions of the selectron in $e^-\gamma \rightarrow \tilde{e}_R^-\tilde{G}$ for $m_{3/2} = 10^{-13}$ GeV and $m_{\tilde{e}_R} = 300$ GeV are shown, where the scattering angle θ is defined from the momentum direction of the incident electron in the $e\gamma$ CM frame. We fix the $e\gamma$ CM energy as $\sqrt{s} = \sqrt{x_{\max} s_{ee}}$, where the photon luminosity sharply peaks for $P_e P_l \sim -1$ (see Fig. 8), i.e. 455 GeV for a 500 GeV collider (left) and 910 GeV for a 1 TeV collider (right). One can find that not only the total cross section as shown in Fig. 9 but also the angular distribution is quite sensitive to the mass of the t -channel intermediate neutralinos. As the neutralino mass is increasing, the cross section with $\lambda_2 = +1$ becomes larger and the peak is shifted to the backward since the t -channel amplitude becomes more important

σ [fb]		$P_{e^-} =$	0	0.9
$\sqrt{s_{ee}} = 500$ GeV	$m_{\tilde{\chi}} = 400$ GeV		5	9
	800 GeV		9	16
	1200 GeV		10	18
	SM background		2594	284
$\sqrt{s_{ee}} = 1$ TeV	$m_{\tilde{\chi}} = 400$ GeV		58	110
	800 GeV		152	289
	1200 GeV		220	416
	SM background		2796	290

Table 4. Cross sections in fb unit for the signal, $e^-\gamma \rightarrow \tilde{e}_R \tilde{G} \rightarrow e^-\tilde{G}\tilde{G}$, and the SM background, $e^-\gamma \rightarrow e^-\nu\bar{\nu}$, at $\sqrt{s_{ee}} = 500$ GeV and 1 TeV without and with the electron beam polarization $P_{e^-} = 0.9$. We take $m_{3/2} = 10^{-13}$ GeV, $m_{\tilde{e}_R} = 300$ GeV, and $B(\tilde{e}_R \rightarrow e\tilde{G}) = 1$. The minimal cuts in (35) and the Z-peak cut in (36) are taken into account.

and its intrinsic $\sin \frac{\theta}{2}$ angular dependence is revealed as $1/(t - m_{\tilde{\chi}}^2)$ goes to $1/m_{\tilde{\chi}}^2$. On the other hand, the cross section with $\lambda_2 = -1$ becomes smaller. As easily seen in Table 3, the productions to the forward region ($\cos \theta = 1$) are forbidden for all helicity combinations because of the angular momentum conservation, while the productions to the backward region ($\cos \theta = -1$) are allowed only for the $\lambda_2 = +1$ case.

Let us now turn to the simulations for the signal of single-electron plus missing energy in the e^+e^- laboratory frame. The partial decay rate of the selectron decay into an electron and a gravitino is given by

$$\Gamma(\tilde{e}_R \rightarrow e\tilde{G}) = \frac{m_{\tilde{e}_R}^5}{48\pi \overline{M}_{\text{Pl}}^2 m_{3/2}^2}, \quad (34)$$

and $\Gamma(\tilde{e}_R \rightarrow e\tilde{G}) = 0.27$ GeV with $m_{\tilde{e}_R} = 300$ GeV and $m_{3/2} = 10^{-13}$ GeV. An irreducible SM background for the event of mono-electron plus missing energy comes from $e^-\gamma \rightarrow e^-\nu\bar{\nu}$. In addition to the minimal cuts for the detection of electrons

$$E_e > 0.03 \sqrt{s}, \quad |\eta_e| < 2, \quad (35)$$

we impose the Z-peak cut

$$M_{\text{miss}} > 100 \text{ GeV}, \quad (36)$$

which can remove the contributions from $e^-\gamma \rightarrow e^-Z \rightarrow e^-\nu\bar{\nu}$. The main background contribution coming from the W -exchange can be reduced by using a polarized electron beam.

In Table 4, the selection efficiencies for the signal and background processes without and with the electron beam polarization are presented, where the above two kinematical cuts, (35) and (36), are taken into account and it is assumed that the branching ratio of the selectron decay to an electron and a gravitino is unity, $B(\tilde{e}_R \rightarrow e\tilde{G}) = 1$. The cross sections both for the signal and background are calculated by MG/MEv4 [21] with gravitino interactions [17, 22], where we also implemented the photon luminosity function of (30). By using a positively polarized electron beam of $P_{e^-} = 0.9$, the signal is enhanced by a factor of

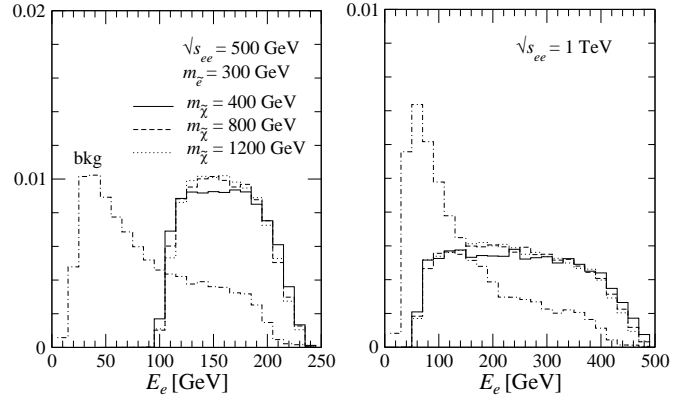


Fig. 11. Normalized energy distributions of the electron for $e^-\gamma \rightarrow \tilde{e}_R \tilde{G} \rightarrow e^-\tilde{G}\tilde{G}$ at $\sqrt{s_{ee}} = 500$ GeV (left) and 1 TeV (right), where $m_{\tilde{\chi}} = 400$ (solid), 800 (dashed) and 1200 (dotted) GeV with $m_{\tilde{e}_R} = 300$ GeV are considered. The kinematical cuts in (35) and (36) and the electron beam polarization $P_{e^-} = 0.9$ are taken into account. Those of the SM background are also shown by dot-dashed lines.

1.9 because the cross section with $\lambda_1 = -1$ is zero, while the background can be reduced by a factor of 10. It must be noted again that the signal cross section is inversely proportional to the gravitino mass squared.

Figure 11 presents normalized energy distributions of the electron for the signal and the SM background, corresponding to 20,000 events each, at $\sqrt{s_{ee}} = 500$ GeV (left) and 1 TeV (right), where the lightest neutralino mass of 400, 800 and 1200 GeV with the 300 GeV selectron mass are considered. The kinematical cuts in (35) and (36) and the electron beam polarization $P_{e^-} = 0.9$ are taken into account. We notice again that the electron distribution is given by two boost effects, along the momentum of the decaying selectron and along the beam axis. The momentum of the incident electron is chosen to the $+z$ direction, and hence the produced electrons in the $e\gamma$ CM frame are boosted to the forward direction. Although the signal distributions no longer have either a flat shape or a sharp edge due to the boost along the beam direction, the energy is restricted as

$$\frac{m_{\tilde{e}_R}^2}{2\sqrt{s_{ee}}} < E_\gamma < \frac{\sqrt{s_{ee}}}{2}, \quad (37)$$

where the lower edge can determine the selectron mass. The energetic electrons tend to be suppressed since the original electron productions in the forward region are not allowed. Moreover, the z -axis boost effect makes the distributions slightly different for the different neutralino mass, which can be dictated by the peak shift in Fig. 10. Since the background is located mostly in the low-energy region, a certain amount of the energy cut can help to enhance the signal over the background.

Finally, the angular distributions of the electron are shown in Fig. 12, where the angle θ_e is measured from the direction of the electron beam, or the $+z$ direction, in the e^+e^- laboratory frame. The electrons tend to be produced more in the forward region ($\cos \theta_e > 0$) due to

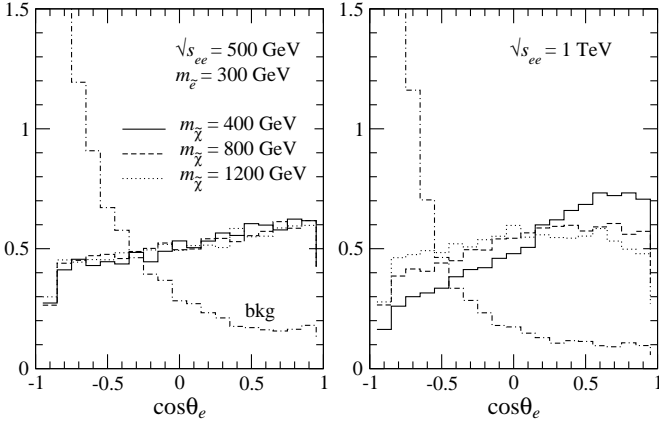


Fig. 12. Normalized angular distributions of the electron in the e^-e^- laboratory frame for $e^-\gamma \rightarrow \tilde{e}_R^-\tilde{G} \rightarrow e^-\tilde{G}\tilde{G}$. The detail is the same as Fig. 11.

the system boost. For the $\sqrt{s_{ee}} = 500$ GeV case the original $m_{\tilde{\chi}}$ dependence in the angular distributions of the selectron shown in Fig. 10 is no longer observed, while the dependence can be seen at $\sqrt{s_{ee}} = 1$ TeV. This indicates that we would be able to determine the mass of the t -channel neutralinos when the collider energy is relatively higher than the selectron mass. We note that the background can be reduced further by a kinematical cut on the backward region.

Before closing this section, we point out that selectron-neutralino associated productions in neutralino LSP scenarios lead to the same signal, or $e + \cancel{E}$, and have been studied intensively [29,30,31,32]. Since the LSP mass is quite different between the two models, $\mathcal{O}(\text{eV})$ for the \tilde{G} LSP and $\mathcal{O}(100 \text{ GeV})$ for the $\tilde{\chi}_1^0$ LSP, the distributions of the final electron are distinctive and could provide a hint of SUSY breaking mechanism.

4 Summary

Associated gravitino productions with a SUSY particle can be observed in current and future collider experiments if the gravitino is very light. In this paper, we restudied the two associated-gravitino-production processes for a future $e^+e^-/e^-\gamma$ collider by using the gravitino implemented **MadGraph/MadEvent**.

First, we studied gravitino productions in association with a neutralino which promptly decays into a photon and a gravitino at an e^+e^- collider, $e^+e^- \rightarrow \tilde{\chi}_1^0\tilde{G} \rightarrow \gamma\tilde{G}\tilde{G}$. By using the effective goldstino interaction Lagrangian we explicitly presented the helicity amplitudes for the production process, which give us deep understanding for the threshold behavior and the SUSY-mass dependence of the production cross section and the angular distributions. We also examined selection efficiencies by kinematical cuts and beam polarizations for the signal and SM background processes, and showed that the energy and angular distributions of the photon in the final state can explore the mass of the t -channel exchange selectrons as well as the mass of the decaying neutralino.

Second, we considered gravitino productions associated with a selectron which subsequently decays into an electron and a gravitino at an $e^-\gamma$ collider, $e^-\gamma \rightarrow \tilde{e}^-\tilde{G} \rightarrow e^-\tilde{G}\tilde{G}$. We repeated the same analyses as in the first process; we presented the explicit helicity amplitudes for the production process, and discussed the mono-electron plus missing-energy signal, including the energy spectrum of the backward-Compton scattered photons for incident photons. Similar to the $e^+e^- \rightarrow \tilde{\chi}_1^0\tilde{G}$ process, we found that the production cross section and the kinematical distributions of the electron in the final state are quite sensitive to the mass of the t -channel intermediate neutralinos as well as the mass of the decaying selectron.

We finally note that, throughout our study, we carefully checked our calculations with the previous works both analytically and numerically, and pointed out a few disagreements.

Before closing, we recall that all the helicity amplitudes we presented are easily applicable to $q\bar{q} \rightarrow \tilde{g}\tilde{G}$ and to $qg \rightarrow \tilde{q}\tilde{G}$ subprocesses for hadron colliders.

Acknowledgements We wish to thank Alberto Mariotti for valuable discussions and comments. We also thank Fabio Maltoni and the members of the CP3, U. Catholique de Louvain for their warm hospitality, where part of this work has been done. The work presented here has been in part supported by the Concerted Research action ‘‘Supersymmetric Models and their Signatures at the Large Hadron Collider’’ of the Vrije Universiteit Brussel, by the Belgian Federal Science Policy Office through the Interuniversity Attraction Pole IAP VI/11, and by the Grant-in-Aid for Scientific Research (No. 20340064) from the Japan Society for the Promotion of Science.

A Effective goldstino interaction Lagrangian

We briefly present the relevant terms of the interaction Lagrangian for our study. The effective goldstino interaction Lagrangian among goldstino, electron and selectron, \tilde{G} - e - \tilde{e}_\pm , and among goldstino, neutralino and photon/ Z -boson, \tilde{G} - $\tilde{\chi}_i^0$ - $V(=\gamma/Z)$, in non-derivative form is

$$\begin{aligned} \mathcal{L}_{\tilde{G}} = & \mp \frac{im_{\tilde{e}_\pm}^2}{\sqrt{3}\overline{M}_{\text{Pl}}m_{3/2}} [\bar{\psi}_{\tilde{G}}P_\pm\psi_e\phi_{\tilde{e}_\pm}^* - \bar{\psi}_eP_\mp\psi_{\tilde{G}}\phi_{\tilde{e}_\pm}] \\ & - \frac{C^{V\tilde{\chi}_i}m_{\tilde{\chi}_i^0}}{4\sqrt{6}\overline{M}_{\text{Pl}}m_{3/2}} \bar{\psi}_{\tilde{G}}[\gamma^\mu, \gamma^\nu]\psi_{\tilde{\chi}_i^0}(\partial_\mu V_\nu - \partial_\nu V_\mu), \end{aligned} \quad (38)$$

where \tilde{e}_\pm denotes the right-/left-handed selectron, $P_\pm = \frac{1}{2}(1 \pm \gamma_5)$ is the chiral-projection operator, and the coupling $C^{V\tilde{\chi}_i}$ is defined in (10); see more details in [22]. All other relevant terms are

$$\mathcal{L}_{eeV} = e\bar{\psi}_e\gamma^\mu[A_\mu - (g_+P_+ + g_-P_-)Z_\mu]\psi_e, \quad (39)$$

$$\mathcal{L}_{\tilde{\chi}_i^0e\tilde{e}} = \pm\sqrt{2}eC_{\pm}^{\tilde{\chi}_i}[\bar{\psi}_{\tilde{\chi}_i^0}P_\pm\psi_e\phi_{\tilde{e}_\pm}^* + \bar{\psi}_eP_\mp\psi_{\tilde{\chi}_i^0}\phi_{\tilde{e}_\pm}], \quad (40)$$

$$\mathcal{L}_{\tilde{e}\tilde{e}\gamma} = ie\phi_{\tilde{e}_\pm}^*\overleftrightarrow{\partial}^\mu\phi_{\tilde{e}_\pm}A_\mu, \quad (41)$$

where g_\pm and $C_{\pm}^{\tilde{\chi}_i}$ are defined in (9) and (10), respectively.

B Helicity amplitudes for $\tilde{\chi}_1^0 \rightarrow \gamma \tilde{G}$

We show helicity amplitudes for the neutralino decay into a photon and a gravitino,

$$\tilde{\chi}_1^0(p_1, \frac{\lambda_1}{2}) \rightarrow \gamma(p_2, \lambda_2) + \tilde{G}(p_3, \frac{\lambda_3}{2}). \quad (42)$$

The partial decay rate in the neutralino rest frame is given by

$$\Gamma = \frac{1}{2m_{\tilde{\chi}_1^0}} \frac{1}{2} \int \sum_{\lambda_1, \lambda_2, \lambda_3} |\mathcal{M}_{\lambda_1, \lambda_2, \lambda_3}|^2 d\Phi_2, \quad (43)$$

and the helicity amplitudes are calculated as

$$\begin{aligned} \mathcal{M}_{+,++} &= -\mathcal{M}_{-,-} = \frac{-C^{\gamma\tilde{\chi}_1} m_{\tilde{\chi}_1^0}^3}{\sqrt{3} \bar{M}_{\text{Pl}} m_{3/2}} \cos \frac{\theta^*}{2}, \\ \mathcal{M}_{+,-} &= \mathcal{M}_{-,+} = \frac{-C^{\gamma\tilde{\chi}_1} m_{\tilde{\chi}_1^0}^3}{\sqrt{3} \bar{M}_{\text{Pl}} m_{3/2}} \sin \frac{\theta^*}{2}, \end{aligned} \quad (44)$$

with $C^{\gamma\tilde{\chi}_1}$ in (10) and the decay angle θ^* defined from the quantization axis of the neutralino spin. The angular dependence is dictated by $J = 1/2$ d functions as

$$\mathcal{M}_{\lambda_1, \lambda_2, \lambda_3} \propto d_{\lambda_1/2, \lambda_2 - \lambda_3/2}^{1/2}(\theta^*). \quad (45)$$

Summing over the initial or final helicities for the amplitudes squared gives the isotropic decay distribution in the rest frame, and one can find the well-known decay rate in Eq. (19).

References

- See, e.g., G. F. Giudice and R. Rattazzi, Phys. Rept. **322** (1999) 419.
- J. R. Ellis, K. Enqvist, D. V. Nanopoulos, Phys. Lett. **B147** (1984) 99; *ibid.* **B151** (1985) 357.
- J. L. Lopez, D. V. Nanopoulos and A. Zichichi, Phys. Rev. D **49** (1994) 343 [arXiv:hep-ph/9210280]; Int. J. Mod. Phys. A **10** (1995) 4241 [arXiv:hep-ph/9408345].
- T. Gherghetta and A. Pomarol, Nucl. Phys. B **586** (2000) 141 [arXiv:hep-ph/0003129]; *ibid.* **B602** (2001) 3-22. [hep-ph/0012378].
- P. Fayet, Phys. Lett. B **175** (1986) 471.
- D. A. Dicus, S. Nandi and J. Woodside, Phys. Lett. B **258** (1991) 231.
- J. L. Lopez, D. V. Nanopoulos and A. Zichichi, Phys. Rev. Lett. **77**, 5168 (1996) [arXiv:hep-ph/9609524].
- J. L. Lopez, D. V. Nanopoulos and A. Zichichi, Phys. Rev. D **55**, 5813 (1997) [arXiv:hep-ph/9611437].
- S. Gopalakrishna and J. D. Wells, Phys. Lett. B **518** (2001) 123 [arXiv:hep-ph/0108006].
- D. A. Dicus, S. Nandi and J. Woodside, Phys. Rev. D **41** (1990) 2347; D. A. Dicus and S. Nandi, Phys. Rev. D **56** (1997) 4166 [arXiv:hep-ph/9611312].
- J. Kim, J. L. Lopez, D. V. Nanopoulos, R. Rangarajan and A. Zichichi, Phys. Rev. D **57** (1998) 373 [arXiv:hep-ph/9707331].
- M. Klasen and G. Pignol, Phys. Rev. D **75** (2007) 115003 [arXiv:hep-ph/0610160].
- J. Abdallah *et al.* [DELPHI Collaboration], Eur. Phys. J. C **38** (2005) 395 [arXiv:hep-ex/0406019].
- D. E. Acosta *et al.* [CDF Collaboration], Phys. Rev. Lett. **89** (2002) 281801 [arXiv:hep-ex/0205057].
- A. A. Affolder *et al.* [CDF Collaboration], Phys. Rev. Lett. **85** (2000) 1378 [arXiv:hep-ex/0003026].
- A. Brignole, F. Feruglio, M. L. Mangano and F. Zwirner, Nucl. Phys. B **526** (1998) 136 [Erratum-*ibid.* B **582** (2000) 759] [arXiv:hep-ph/9801329].
- K. Hagiwara, K. Mawatari and Y. Takaesu, Eur. Phys. J. C **71** (2011) 1529 [arXiv:1010.4255 [hep-ph]].
- K. Hagiwara, H. Murayama and I. Watanabe, Nucl. Phys. B **367** (1991) 257; H. Murayama, I. Watanabe and K. Hagiwara, KEK-Report 91-11, 1992.
- T. Stelzer and W. F. Long, Comput. Phys. Commun. **81** (1994) 357 [arXiv:hep-ph/9401258]; G. C. Cho, K. Hagiwara, J. Kanzaki, T. Plehn, D. Rainwater and T. Stelzer, Phys. Rev. D **73** (2006) 054002 [arXiv:hep-ph/0601063].
- F. Maltoni and T. Stelzer, JHEP **0302** (2003) 027 [arXiv:hep-ph/0208156].
- J. Alwall, P. Demin, S. de Visscher, R. Frederix, M. Herquet, F. Maltoni, T. Plehn, D. Rainwater and T. Stelzer, JHEP **0709** (2007) 028 [arXiv:0706.2334 [hep-ph]]; <http://madgraph.phys.ucl.ac.be/>.
- K. Mawatari and Y. Takaesu, Eur. Phys. J. C **71** (2011) 1640 [arXiv:1101.1289 [hep-ph]].
- J. Brau *et al.* [ILC Collaboration], arXiv:0712.1950 [physics.acc-ph].
- I. F. Ginzburg, G. L. Kotkin, V. G. Serbo and V. I. Telnov, JETP Lett. **34** (1981) 491; I. F. Ginzburg, G. L. Kotkin, V. G. Serbo and V. I. Telnov, Nucl. Instrum. Meth. **205** (1983) 47.
- I. F. Ginzburg, G. L. Kotkin, S. L. Panfil, V. G. Serbo and V. I. Telnov, Nucl. Instrum. Meth. A **219** (1984) 5.
- S. Y. Choi, K. Hagiwara, H. U. Martyn, K. Mawatari and P. M. Zerwas, Eur. Phys. J. C **51**, 753 (2007) [arXiv:hep-ph/0612301].
- S. Ambrosanio and G. A. Blair, Eur. Phys. J. C **12** (2000) 287 [arXiv:hep-ph/9905403].
- B. Badelek *et al.* [ECFA/DESY Photon Collider Working Group], Int. J. Mod. Phys. A **19** (2004) 5097 [arXiv:hep-ex/0108012].
- F. Cuyppers, G. J. van Oldenborgh and R. Ruckl, Nucl. Phys. B **383** (1992) 45 [arXiv:hep-ph/9205209]; H. Konig and K. A. Peterson, Phys. Lett. B **294** (1992) 110 [arXiv:hep-ph/9205201]; T. Kon and A. Goto, Phys. Lett. B **295** (1992) 324.
- D. Choudhury and F. Cuyppers, Nucl. Phys. B **451** (1995) 16 [arXiv:hep-ph/9412245].
- K. Kiers, J. N. Ng and G. h. Wu, Phys. Lett. B **381** (1996) 177 [arXiv:hep-ph/9604338].
- V. D. Barger, T. Han and J. Kelly, Phys. Lett. B **419** (1998) 233 [arXiv:hep-ph/9709366].